Photo double ionization of molecular deuterium

T J Reddish† and J M Feagin‡

† Physics Department, The University of Newcastle, Newcastle upon Tyne NEI 7RU, UK
‡ Department of Physics, California State University-Fullerton, Fullerton, CA 92834, USA

Abstract. A helium-like description of photo double ionization of molecular deuterium is extended to derive a dependence of molecular excitation amplitudes on electron energy sharing and dynamical quantum numbers labelling internal modes of excitation of the escaping electron pair. Both linear and circular polarizations are considered, and predictions regarding circular dichroisms in the angular distributions of the electron and ion pairs are given. A detailed comparison of the model with recent $(\gamma, 2e)$ measurements is also presented.

1. Introduction

Photo double ionization (PDI) of molecular deuterium D_2—or equivalently molecular hydrogen H_2—is challenging because of the inevitable full four-particle fragmentation of the molecule. A thorough study of the resulting few-body escape dynamics clearly requires measurement of *differential* cross sections, particularly for the lowest photon energies. Recent $(\gamma, 2e)$ studies of D_2 (Reddish *et al* 1997a, Wightman *et al* 1998, Scherer *et al* 1998) have demonstrated a remarkable likeness of D_2 and helium triply differential cross sections (TDCS), although the characteristic pair of lobes in the helium distributions are closer together in the molecule and significantly narrower. The two groups' measurements are in excellent agreement and were both obtained for equal electron energy sharing, $E_1 = E_2 \sim 10$ eV, with coplanar detection orthogonal to the photon beam direction. In addition, Dörner *et al* (1998b) have performed coincidence experiments between the ion pairs and one of the escaping electrons. They thus extracted a one-electron angular asymmetry parameter β_1 as a function of electron energy sharing for parallel and perpendicular ion-axis orientations relative to the photon polarization. They also made the surprising observation that the electron distribution is azimuthally symmetric about the photon polarization axis even when the azimuthal symmetry is broken by a perpendicular ion-axis orientation. These experiments have awakened interest in PDI of these fundamental molecules after a decade of silence following the pioneering ion–ion coincidence experiments on H_2 of Dujardin *et al* (1987) and of Kossmann *et al* (1989).

We have recently developed a very basic description of the TDCS for diatomic molecules (Feagin 1998) based closely on the PDI amplitude for helium (e.g. Huetz *et al* 1991, 1995, Lablanquie *et al* 1995, Maulbetsch and Briggs 1993, Kazansky and Ostrovsky 1995, Pont and Shakeshaft 1995, Feagin 1996) and also on the earlier theoretical studies of Le Rouzo (1986, 1988). We thus derive a helium-like expression for the electron-pair angular distribution which depends on the orientation of the ion axis at the instant of photoionization and therefore on amplitudes for excitation parallel and perpendicular to the molecular axis. When integrated over the momentum of an undetected electron for comparison with the ion–electron results of

Dörner *et al* (1998b), we obtain the azimuthally symmetric electron distribution they observed for ion-axis alignments both parallel and perpendicular to the photon polarization axis. When integrated over the alignment of an undetected ion axis for comparison with our $(\gamma, 2e)$ data and also the data of Scherer *et al* (1998), we obtain an expression with two contributions: one identical in form to the helium TDCS; and one with an angular distribution independent of the photon polarization direction and proportional to the square of the difference in amplitudes for parallel and perpendicular molecular excitation. The result is in good agreement with measured ratios of the TDCS in D_2 to that in He and helps to explain a surprising observed increase in the ratios where the individual angular distributions vanish due to an exact parity-exchange selection rule.

In this paper, we extend our earlier derivation of the molecular photofragmentation amplitude (Feagin 1998) to include a fourth-order Wannier description of the electron-pair continuum wavefunction and thereby obtain an approximate E_1, E_2 energy dependence of the amplitudes for excitation parallel and perpendicular to the molecular axis. At the same time, we attempt to exhibit the role of dynamical excitations internal to the electron pair. Berakdar and Klar (1992) predicted, and Viefhaus *et al* (1996) and Mergel *et al* (1998) demonstrated, that PDI in helium with circularly polarized photons leads to a dichroism in the electron-pair angular distribution, and that phase-sensitive probes of the internal electron-pair continuum dynamics are possible (Berakdar *et al* 1993, see also Berakdar 1998, 1999). Thus, we also extend our description of molecular photofragmentation to include dichroism, a topic with a long and rich history in molecular physics, although we focus on the phenomenon as a tool to probe few-body Coulomb dynamics. Finally, we present further technical details on the comparison of our description with measured TDCS ratios in D_2 and He and provide additional experimental evidence for some of the conclusions we have drawn.

Our theoretical description of the outgoing electron pair is characterized by the collective coordinates defined by the separation vector $\boldsymbol{R} = \boldsymbol{r}_1 - \boldsymbol{r}_2$ and the centre-of-mass (CM) position vector $\boldsymbol{r} = \frac{1}{2}(\boldsymbol{r}_1 + \boldsymbol{r}_2)$ of the ionized electron pair relative to the CM of the ion pair. These vectors replace the usual position vectors $\boldsymbol{r}_1$ and $\boldsymbol{r}_2$ of the electrons relative to the ion-pair CM, so that the dipole excitation operator of the electron pair reduces to simply $\boldsymbol{\epsilon} \cdot \boldsymbol{r}_1 + \boldsymbol{\epsilon} \cdot \boldsymbol{r}_2 = 2\boldsymbol{\epsilon} \cdot \boldsymbol{r}$. We thus consider a photon absorbed by the electron-pair CM and describe the fragmentation state of the system by a Wannier *momentum* function of the detector coordinates

$$
\begin{aligned}
\boldsymbol{k}_r &= \boldsymbol{k}_1 + \boldsymbol{k}_2 \qquad \boldsymbol{k}_R = \tfrac{1}{2}(\boldsymbol{k}_1 - \boldsymbol{k}_2) \\
k_r &= 2\sqrt{\tfrac{1}{2}E + \sqrt{E_1 E_2}\cos\theta_{12}} \qquad k_R = \sqrt{\tfrac{1}{2}E - \sqrt{E_1 E_2}\cos\theta_{12}}
\end{aligned}
\tag{1}
$$

conjugate to $\boldsymbol{r}$ and $\boldsymbol{R}$. Here $\boldsymbol{k}_1$ and $\boldsymbol{k}_2$ are the conventional detector coordinates, i.e. the momenta conjugate to $\boldsymbol{r}_1$ and $\boldsymbol{r}_2$, with mutual angle $\theta_{12} = \cos^{-1}(\hat{\boldsymbol{k}}_1 \cdot \hat{\boldsymbol{k}}_2)$ and electron energies $E_i = \frac{1}{2}k_i^2$. Then, $E = E_1 + E_2$ is the system excess energy above threshold, an approximate quantity defined by the 'vertical transition' from the molecular ground state to the ion-exploding continuum state.

We will derive and express our results using vector methods independent of a particular angular representation. Then, to derive the angular dependence of a cross section as a function of $\boldsymbol{k}_r$, $\boldsymbol{k}_R$ or $\boldsymbol{k}_1$, $\boldsymbol{k}_2$, we will only need the polar-angle representation of the momentum vectors relative to *lab-fixed* axes,

$$
\hat{\boldsymbol{k}}_i = \sin\theta_i \cos\phi_i \hat{\boldsymbol{x}} + \sin\theta_i \sin\phi_i \hat{\boldsymbol{y}} + \cos\theta_i \hat{\boldsymbol{z}},
\tag{2}
$$

where i stands for any of the labels R, r, 1 or 2.

We use atomic units throughout, except that we label energies in eV.

2. Photoionization cross section

We retain the axial-recoil description of Feagin (1998) to write down an approximate transition dipole moment describing the excitation and escape of the electron pair from the molecule. We thus assume the ion-axis orientation $\boldsymbol{R}_N$ is fixed during the quick escape of the electrons from the instant of photon absorption to the resulting Coulomb explosion of the ion pair (cf Zare 1988). We will generalize this description, however, to arbitrary electron energy sharing E_1 and $E_2 = E - E_1$ and to include circular dichroism. We thus consider just the Wannier component $\psi^W_{\boldsymbol{k}_r \boldsymbol{k}_R}$ of the electron-pair continuum state $\psi_{\boldsymbol{k}_r \boldsymbol{k}_R}$ which has been photoexcited from an electron-pair initial state ψ_i, and define the components of the *molecular-frame* transition dipole moment according to (primes denote molecular-frame quantities)

$$\mu'_\alpha \equiv \langle \psi_{\boldsymbol{k}'_r \boldsymbol{k}'_R} | x'_\alpha | \psi_i \rangle \simeq \sum_K \langle \psi_{\boldsymbol{k}'_r \boldsymbol{k}'_R} | \psi^W_{LK} \rangle \langle \psi^W_{LK} | x'_\alpha | \psi_i \rangle, \tag{3}$$

where $x'_\alpha = \boldsymbol{r}' \cdot \boldsymbol{\epsilon}'_\alpha$ is a component of the electron-pair CM vector along one of the molecular-frame axes $\alpha = x', y', z'$ with the z' axis along the internuclear axis $\boldsymbol{R}_N$. Here L is the total angular momentum quantum number of the electron pair, while K is its projection quantum number along the interelectronic momentum direction $\hat{\boldsymbol{k}}_R$, $|\boldsymbol{L} \cdot \hat{\boldsymbol{k}}_R| \equiv K$. Once we have rotated the dipole moment from the molecular frame to the laboratory frame $\mu' \to \mu$, we obtain the molecular PDI amplitude from simply $f(\boldsymbol{R}_N) = \boldsymbol{\epsilon} \cdot \boldsymbol{\mu}$ for a given photon polarization $\boldsymbol{\epsilon}$.

If we take the final state $\langle \psi_{\boldsymbol{k}'_r \boldsymbol{k}'_R} |$ to be simply an outgoing plane-wave detector state, then the overlap $\langle \psi_{\boldsymbol{k}'_r \boldsymbol{k}'_R} | \psi^W_{LK} \rangle \simeq \tilde{\psi}^W_{LK}(\boldsymbol{k}'_r, \boldsymbol{k}'_R)$, i.e. the momentum-space representation (Fourier transform) of the Wannier wavefunction. This momentum wavefunction then characterizes for us the dependence of the cross section on the detector coordinates $\boldsymbol{k}_r$ and $\boldsymbol{k}_R$. In particular, the *internal* excitation amplitudes $c_{\alpha K} \equiv \langle \psi^W_{LK} | x'_\alpha | \psi_i \rangle$ from equation (3) depend only on the excess energy E—fully independent of the momenta $\boldsymbol{k}_r$ and $\boldsymbol{k}_R$. The rotational symmetry of the diatomic molecule about $\boldsymbol{R}_N$ requires that $c_{x'K} = c_{y'K} \equiv c_{\Pi K}$ and $c_{z'K} \equiv c_{\Sigma K}$, where Σ and Π are the conventional labels distinguishing excitations parallel and perpendicular, respectively, to the molecular axis. In a partial-wave analysis, Σ and Π also specify *perpendicular* and *parallel* projections, respectively, of the electron-pair angular momentum along the molecular axis, $|\boldsymbol{L} \cdot \hat{\boldsymbol{R}}_N|$. In principle, these amplitudes contain all initial state effects and the gauge dependence. Rather than evaluate them here, however, we simply parametrize our results in terms of their ratios.

Following Feagin (1998), we approximate $\tilde{\psi}^W_{LK}(\boldsymbol{k}'_r, \boldsymbol{k}'_R)$ by the helium $^1\mathrm{P}^{\mathrm{o}}$ momentum distribution so that $K = 0, 1$ and thereby consider excitation of the dominant $^1\mathrm{S}^{\mathrm{e}}$ component of the molecular ground state†. We thus obtain from fourth-order Wannier theory the simple and useful geometrical form (see Feagin 1995, 1996, and also Dörner *et al* 1998a)

$$\tilde{\psi}^W_{L=1,K}(\boldsymbol{k}'_r, \boldsymbol{k}'_R) \sim \tilde{\Lambda}(k_r, k_R) \times \begin{cases} -\boldsymbol{\epsilon}'_\alpha \cdot \hat{\boldsymbol{k}}'_R \hat{\boldsymbol{k}}'_R \cdot \boldsymbol{k}'_r, & K = 0 \\ \boldsymbol{\epsilon}'_\alpha \cdot \boldsymbol{k}'_r - \boldsymbol{\epsilon}'_\alpha \cdot \hat{\boldsymbol{k}}'_R \hat{\boldsymbol{k}}'_R \cdot \boldsymbol{k}'_r, & K = 1, \end{cases} \tag{4}$$

where $\tilde{\Lambda}(k_r, k_R)$ is an 'internal' momentum wavefunction. With this approximation the molecular transition dipole moment equation (3) has the simple and useful form

$$\mu'_\alpha \simeq \tilde{\Lambda}(k_r, k_R) \left(c_{\alpha 1} \boldsymbol{\epsilon}'_\alpha \cdot \boldsymbol{k}'_r - (c_{\alpha 0} + c_{\alpha 1}) \boldsymbol{\epsilon}'_\alpha \cdot \hat{\boldsymbol{k}}'_R \hat{\boldsymbol{k}}'_R \cdot \boldsymbol{k}'_r \right), \tag{5}$$

so that if we define a diagonal dyadic C'_K with diagonal components $c_{x'K} = c_{y'K} = c_{\Pi K}$ and $c_{z'K} = c_{\Sigma K}$, the molecular-frame *vector* dipole moment can be written conveniently as

$$\boldsymbol{\mu}' \simeq \tilde{\Lambda}(k_r, k_R) \left(C'_1 \cdot \boldsymbol{k}'_r - (C'_0 + C'_1) \cdot \hat{\boldsymbol{k}}'_R \hat{\boldsymbol{k}}'_R \cdot \boldsymbol{k}'_r \right). \tag{6}$$

---

† Joy and Parr (1958) estimated the ground state components to be 95.8% s^2 S^e, 2.6% sd D^e, and 1.5% p^2. See also Bishop (1963).

This notation facilitates rotation to the laboratory frame. The transformation is readily accomplished without reference to Euler angles by noting that the molecular-frame diagonal dyadic C'_K can be expressed as $C'_K = c_{\Pi K}\mathsf{I} + (c_{\Sigma K} - c_{\Pi K})\hat{R}'_N\hat{R}'_N$, where I is the unit dyad. Then, since $\hat{R}'_N \to \hat{R}_N$ under rotation to the lab frame, $C'_K \to C_K = c_{\Pi K}\mathsf{I} + (c_{\Sigma K} - c_{\Pi K})\hat{R}_N\hat{R}_N$ under rotation. (Despite the form invariance, C_K is nondiagonal.) It follows that the lab-frame dipole moment $\boldsymbol{\mu}$ is form invariant under rotation with all vectors in equation (6) simply replaced by their 'unprimed' lab-frame counterparts. Hence, the molecular photoexcitation amplitude for linear polarization $\boldsymbol{\epsilon}$ is given by

$$
\begin{aligned}
f(\boldsymbol{R}_N) = \boldsymbol{\epsilon}\cdot\boldsymbol{\mu} &\simeq \tilde{\Lambda}(k_r, k_R)\Big[\boldsymbol{\epsilon}\cdot\boldsymbol{C}_1\cdot\boldsymbol{k}_r - \boldsymbol{\epsilon}\cdot(\boldsymbol{C}_0+\boldsymbol{C}_1)\cdot\hat{\boldsymbol{k}}_R\hat{\boldsymbol{k}}_R\cdot\boldsymbol{k}_r\Big] \\
&= \tilde{\Lambda}(k_r, k_R)\Big[c_{\Pi 1}\boldsymbol{\epsilon}\cdot\boldsymbol{k}_r - (c_{\Pi 0}+c_{\Pi 1})\boldsymbol{\epsilon}\cdot\hat{\boldsymbol{k}}_R\hat{\boldsymbol{k}}_R\cdot\boldsymbol{k}_r \\
&\quad + \boldsymbol{\epsilon}\cdot\hat{\boldsymbol{R}}_N\Big(\Delta c_1\hat{\boldsymbol{R}}_N\cdot\boldsymbol{k}_r - (\Delta c_0+\Delta c_1)\hat{\boldsymbol{R}}_N\cdot\hat{\boldsymbol{k}}_R\hat{\boldsymbol{k}}_R\cdot\boldsymbol{k}_r\Big)\Big]
\end{aligned}
\tag{7}
$$

where $\Delta c_K \equiv c_{\Sigma K} - c_{\Pi K}$. We consider circular polarization below. The scalar product $\hat{\boldsymbol{k}}_R\cdot\boldsymbol{k}_r$ in this result makes clear that detecting $\boldsymbol{k}_R\perp\boldsymbol{k}_r$ selects *pure $K = 1$* internal excitation. On the other hand, detecting $\boldsymbol{k}_R\|\boldsymbol{k}_r$ selects *pure $K = 0$* internal excitation. In general, the electron pair occupies a $K = 0, 1$ mixture, although we might expect from studies of helium (Dörner *et al* 1998a) in the 1–20 eV range that the $K = 1$ amplitudes dominate by roughly a factor of three. Likewise, detecting $\boldsymbol{R}_N\perp\boldsymbol{\epsilon}$ selects *pure Π* molecular excitation, whereas detecting $\boldsymbol{R}_N\|\boldsymbol{\epsilon}$ selects *pure Σ* molecular excitation. As expected, equation (7) reduces to the helium PDI amplitude (cf Dörner *et al* 1998b) if one ignores Σ, Π differences and sets $c_{\Sigma K} = c_{\Pi K} = c_K$.

Equation (7) is easily transformed to conventional detector coordinates $\boldsymbol{k}_1$ and $\boldsymbol{k}_2$ using equation (1). We thus recover not only the photoexcitation amplitude derived in Feagin (1998),

$$
f(\boldsymbol{R}_N) = \boldsymbol{\epsilon}\cdot\boldsymbol{\mu} = \boldsymbol{\epsilon}\cdot\mathbf{g}(1, 2, \theta_{12})\cdot\hat{\boldsymbol{k}}_1 + \boldsymbol{\epsilon}\cdot\mathbf{g}(2, 1, \theta_{12})\cdot\hat{\boldsymbol{k}}_2,
\tag{8}
$$

where the dyadics are defined as $\mathbf{g} = g_\Pi\mathsf{I} + (g_\Sigma - g_\Pi)\hat{\boldsymbol{R}}_N\hat{\boldsymbol{R}}_N$, but also derive an approximate dependence of the amplitudes g_Σ, g_Π on the electron-pair energy sharing,

$$
g_\alpha(i, j, \theta_{12}) \simeq \tilde{\Lambda}(E_1, E_2, \theta_{12})\sqrt{2E_i}\left[c_{\alpha 1} - \frac{E_i - E_j}{2k_R^2}(c_{\alpha 0} + c_{\alpha 1})\right].
\tag{9}
$$

(Note, $k_R^2 = \frac{1}{2}E - \sqrt{E_1 E_2}\cos\theta_{12}$ from equation (1).) As discussed above, detecting either $\boldsymbol{R}_N\|\boldsymbol{\epsilon}$ or $\boldsymbol{R}_N\perp\boldsymbol{\epsilon}$ reduces $f(\boldsymbol{R}_N)$ to a helium-like amplitude, either $f \to g_\Sigma(1, 2, \theta_{12})\boldsymbol{\epsilon}\cdot\hat{\boldsymbol{k}}_1 + g_\Sigma(2, 1, \theta_{12})\boldsymbol{\epsilon}\cdot\hat{\boldsymbol{k}}_2$ or $f \to g_\Pi(1, 2, \theta_{12})\boldsymbol{\epsilon}\cdot\hat{\boldsymbol{k}}_1 + g_\Pi(2, 1, \theta_{12})\boldsymbol{\epsilon}\cdot\hat{\boldsymbol{k}}_2$. Both of these limits display azimuthal symmetry about the polarization axis $\boldsymbol{\epsilon}$. Although the $\boldsymbol{R}_N\|\boldsymbol{\epsilon}$ limit is expected when the azimuthally symmetric initial state is aligned along $\boldsymbol{\epsilon}$, the $\boldsymbol{R}_N\perp\boldsymbol{\epsilon}$ limit is at first surprising since the azimuthal symmetry is broken by the initial-state alignment. This result is of course just an artifact of our description which considers excitation of only the dominant $^1S^e$ ground-state component. Nevertheless, the recent measurements of Dörner *et al* (1998b) support our $\boldsymbol{R}_N\perp\boldsymbol{\epsilon}$ limit.

Equations (7)–(9) give the correct kinematic dependence on the electron-pair *vector* momenta for a helium-like $^1S^e \to {}^1P^o$ transition, although the internal wavefunction $\tilde{\Lambda}(k_r, k_R) \equiv \tilde{\Lambda}(E_1, E_2, \theta_{12})$ has not been derived for molecular fragmentation. The dynamical Wannier saddle in the presence of the molecular axis is too complicated to warrant using the fourth-order internal wavefunction derived for helium (Feagin 1995, 1996, see also Dörner *et al* 1998a). We therefore simply replace the internal wavefunction with the conventional Gaussian 'correlation function' predicted by second-order Wannier theory in helium. Namely,

we use

$$|\tilde{\Lambda}(E_1, E_2, \theta_{12})|^2 \equiv G(E, \theta_{12}) \sim \exp\left(-4\ln 2 \frac{(\pi - \theta_{12})^2}{\theta_{1/2}^2(E)}\right) \tag{10}$$

with half-width $\theta_{1/2}(E)$. In the case of equal-energy sharing, this result has proven extremely useful in parametrizing a variety of helium data even tens of eV above threshold. The Gaussian wavefunction is a consequence of the harmonic bending motion of the electron pair relative to the ion charge centre, a feature shared by both the atomic and the molecular potentials in lowest order. Although we will not do so here, one might introduce separate correlation functions G_Σ and G_Π with differing half-widths for parallel and perpendicular excitations (cf Dörner *et al* 1998b).

The square of the excitation amplitude $|f(\boldsymbol{R}_N)|^2$ determines the four-body fragmentation distributions. For example, if we integrate over all ion-axis alignments $\hat{\boldsymbol{R}}_N$, we derive a TDCS for just the electron pair relevant to the experiments discussed in section 4. (The cross section is in fact quadruply differential because the Coulomb exploding ions have a small 'Franck–Condon' spread in energy of 2–3 eV.) The integration over $\hat{\boldsymbol{R}}_N$ is straightforward with the two identities $\int \hat{\boldsymbol{R}}_N \hat{\boldsymbol{R}}_N \, \mathrm{d}\hat{\boldsymbol{R}}_N = \frac{4\pi}{3}\mathbf{I}$ and $\int(\boldsymbol{\epsilon} \cdot \hat{\boldsymbol{R}}_N)^2 \hat{\boldsymbol{R}}_N \hat{\boldsymbol{R}}_N \, \mathrm{d}\hat{\boldsymbol{R}}_N = \frac{4\pi}{15}(\mathbf{I} + 2\boldsymbol{\epsilon}\boldsymbol{\epsilon})$. We thus generalize Feagin (1998) again to arbitrary electron-pair energy sharing according to

$$\begin{aligned}
\mathrm{TDCS}[\mathrm{D}_2] &\sim \int |\boldsymbol{\epsilon} \cdot \boldsymbol{\mu}|^2 \frac{\mathrm{d}\hat{\boldsymbol{R}}_N}{4\pi} \\
&= \tfrac{2}{15}|g_\Sigma(1, 2, \theta_{12})\boldsymbol{\epsilon} \cdot \hat{\boldsymbol{k}}_1 + g_\Sigma(2, 1, \theta_{12})\boldsymbol{\epsilon} \cdot \hat{\boldsymbol{k}}_2|^2 \\
&\quad + \tfrac{7}{15}|g_\Pi(1, 2, \theta_{12})\boldsymbol{\epsilon} \cdot \hat{\boldsymbol{k}}_1 + g_\Pi(2, 1, \theta_{12})\boldsymbol{\epsilon} \cdot \hat{\boldsymbol{k}}_2|^2 \\
&\quad + \tfrac{6}{15}\mathrm{Re}\left([g_\Sigma^*(1, 2, \theta_{12})\boldsymbol{\epsilon} \cdot \hat{\boldsymbol{k}}_1 + g_\Sigma^*(2, 1, \theta_{12})\boldsymbol{\epsilon} \cdot \hat{\boldsymbol{k}}_2]\right. \\
&\quad\quad\quad \left.\times [g_\Pi(1, 2, \theta_{12})\boldsymbol{\epsilon} \cdot \hat{\boldsymbol{k}}_1 + g_\Pi(2, 1, \theta_{12})\boldsymbol{\epsilon} \cdot \hat{\boldsymbol{k}}_2]\right) \\
&\quad + \tfrac{1}{15}|\Delta g(1, 2, \theta_{12})\hat{\boldsymbol{k}}_1 + \Delta g(2, 1, \theta_{12})\hat{\boldsymbol{k}}_2|^2, \tag{11}
\end{aligned}$$

where $\Delta g \equiv g_\Sigma - g_\Pi$. In the limit $g_\Sigma \to g_\Pi$, this result reduces as expected to the helium cross section $\mathrm{TDCS}[\mathrm{He}] = |g(1, 2, \theta_{12})\boldsymbol{\epsilon} \cdot \hat{\boldsymbol{k}}_1 + g(2, 1, \theta_{12})\boldsymbol{\epsilon} \cdot \hat{\boldsymbol{k}}_2|^2$.

We derive doubly differential cross sections (DDCS) for a single electron by integrating the square of the excitation amplitude $|f(\boldsymbol{R}_N)|^2$ from equation (8) or the TDCS from equation (11) over *either* $\hat{\boldsymbol{k}}_1$ or $\hat{\boldsymbol{k}}_2$. For example, starting with equation (11) and integrating over $\hat{\boldsymbol{k}}_2$, we derive the familiar form

$$\frac{\mathrm{d}^2\sigma}{\mathrm{d}E_1 \, \mathrm{d}\hat{\boldsymbol{k}}_1} = \frac{1}{4\pi}\frac{\mathrm{d}\sigma}{\mathrm{d}E_1}\left(1 + \beta_1 P_2(\boldsymbol{\epsilon} \cdot \hat{\boldsymbol{k}}_1)\right), \tag{12}$$

where $P_2(\boldsymbol{\epsilon} \cdot \hat{\boldsymbol{k}}_1)$ is a second-order Legendre polynomial and β_1 the angular asymmetry parameter. On the other hand, the $\boldsymbol{R}_N$-dependent DDCS derived from the square of the excitation amplitude $|f(\boldsymbol{R}_N)|^2$ from equation (8) can be generally expressed in terms of $P_2(\boldsymbol{\epsilon} \cdot \hat{\boldsymbol{k}}_1)$ for only the two special geometries $\boldsymbol{R}_N \| \boldsymbol{\epsilon}$ or $\boldsymbol{R}_N \perp \boldsymbol{\epsilon}$. The former limit is a general result, while the latter is a consequence of our model. In any case, detailed evaluation of β_1 requires a numerical integration because of the complicated angular dependence of the amplitudes $g_\alpha(i, j, \theta_{12})$ (see Dörner *et al* 1998b).

We derive an *ion* angular distribution by integrating the square of the excitation amplitude $|f(\boldsymbol{R}_N)|^2$ from equation (8) over *both* $\hat{\boldsymbol{k}}_1$ and $\hat{\boldsymbol{k}}_2$, although it is more straightforward to start with $|f(\boldsymbol{R}_N)|^2$ from equation (7) and integrate over $\hat{\boldsymbol{k}}_r$ and $\hat{\boldsymbol{k}}_R$. Again, detailed evaluation requires numerical integration. We can derive, however, a useful approximate expression for

the ion angular asymmetry parameter β_N by ignoring the weaker angular dependence of the correlation function $G(E, \theta_{12})$. The integrals are then easily performed with one of the dyadic identities introduced above equation (11), $\int \hat{k}_i \hat{k}_i \, d\hat{k}_i = \frac{4\pi}{3} \mathbf{I}$, and with some rearrangement we obtain the familiar form (Dehmer and Dill 1978),

$$\frac{d\sigma}{d\hat{R}_N} \propto |\epsilon \cdot C_0|^2 + 2|\epsilon \cdot C_1|^2 \sim 1 + \beta_N P_2(\epsilon \cdot \hat{R}_N) \tag{13}$$

where $\beta_N = 2(D_\Sigma^2 - D_\Pi^2)/(D_\Sigma^2 + 2D_\Pi^2)$ but now $D_\alpha^2 \equiv |c_{\alpha 0}|^2 + 2|c_{\alpha 1}|^2$. We compare this quantity with experiment in section 4.

3. Circular dichroism

If the absorbed photon is circularly polarized then changing the polarization from left to right $\epsilon_+ \rightarrow \epsilon_-$ is tantamount to reflecting the system in a vertical plane passing through the photon propagation direction $\hat{k}_\gamma$, which we take to be the laboratory $\hat{z}$ axis with $\epsilon_\pm = \frac{1}{\sqrt{2}}(\hat{x} \pm i\hat{y})$. Consider the unitary reflection operator defined by

$$\sigma_v |\hat{x}, \hat{y}, \hat{z}\rangle = |\hat{x}, -\hat{y}, \hat{z}\rangle \tag{14}$$

under which the dipole excitation operator transforms according to ($\sigma_v^\dagger$ denotes adjoint)

$$\epsilon_+ \cdot r = \sigma_v \epsilon_- \cdot r \sigma_v^\dagger. \tag{15}$$

If we reflect for simplicity in the vertical plane defined by k_γ and the molecular axis R_N, then the electron-pair initial state is unchanged under reflection, $\sigma_v |\psi_i(\hat{R}_N)\rangle = |\psi_i(\hat{R}_N)\rangle$, and the dipole excitation amplitude transforms as

$$f_M(k_r, k_R, \hat{R}_N) = \langle \psi_{k_r, k_R}(\hat{R}_N)|\epsilon_M \cdot r|\psi_i(\hat{R}_N)\rangle$$
$$= \langle \psi_{k_r', k_R'}(\hat{R}_N)|\epsilon_{-M} \cdot r|\psi_i(\hat{R}_N)\rangle = f_{-M}(k_r', k_R', \hat{R}_N). \tag{16}$$

Here k_r' and k_R' are the momentum vectors expressed along the reflected coordinate axes and therefore with components $\{k_x', k_y', k_z'\} = \{k_x, -k_y, k_z\}$. Thus, changing the circular polarization reflects the cross section in the $\hat{x}$, $\hat{z}$ plane, and equation (16) relates momentum-space points on opposite sides of the plane. Of course, this result is not due to any intrinsic chirality of molecular deuterium. Rather, the chirality of the photon is transferred to the electron and ion pairs.

It is also clear that one requires at least three distinct directions to establish a handedness, say k_γ and two of the three vectors k_R, k_r, R_N, or k_1, k_2, R_N. Otherwise, the reflection is degenerate with a rotational symmetry. For example, if one detects just k_1 and k_2, but $k_1 = k_2$, or if all three vectors k_1, k_2, and k_γ lie in the same plane, then any reflection σ_v can also be generated by a rotation about k_γ. Likewise, states with k_R perpendicular to k_r are also reflection–rotation degenerate. This case corresponds again to $k_1 = k_2$, since $k_r \cdot k_R = E_1 - E_2$ from equation (1). These degeneracies apply to helium as well as to molecular deuterium. However, note that in helium one must detect both electrons to observe dichroism, whereas in the molecule one could detect instead one of the ions and just one of the electrons. In addition, ion-exchange symmetry in D_2 simply means that the cross sections are symmetric with respect to $R_N \rightarrow -R_N$, analogous to the symmetry of singlet electron-pair states under electron exchange $k_R \rightarrow -k_R$ in both the atom and the molecule. For example, photofragmentation of molecular HD would break this symmetry, though the effect would be very weak.

The dichroism arises from the fact that $|f_{+1}(k_r, k_R, R_N)|^2 - |f_{-1}(k_r, k_R, R_N)|^2$ is generally nonvanishing, despite the reflection symmetry equation (16). (Note here one

compares momentum points on the same side of the reflection plane.) Physically, the dichroism means that the photon absorption rate and the resulting electron–ion or electron-pair detection rates will differ if the ion and electron detectors are held fixed and the circular polarization changed. We now relate this fact to coherent excitation of distinct dynamical symmetries.

With the excitation amplitude written as $f_M = \epsilon_M \cdot \mu$, the dichroism is defined by

$$\Delta(\mathbf{R}_N) \equiv |f_{+1}(\mathbf{k}_r, \mathbf{k}_R, \mathbf{R}_N)|^2 - |f_{-1}(\mathbf{k}_r, \mathbf{k}_R, \mathbf{R}_N)|^2$$
$$= \mu^* \cdot (\epsilon_+^* \epsilon_+ - \epsilon_-^* \epsilon_-) \cdot \mu. \tag{17}$$

This expression is conveniently evaluated in terms of the dyadic

$$\epsilon_M^* \epsilon_M = \tfrac{1}{2}[\hat{x}\hat{x} + \hat{y}\hat{y} + i^M(\hat{x}\hat{y} - \hat{y}\hat{x})]. \tag{18}$$

The cross term antisymmetric under reflection $\hat{y} \to -\hat{y}$ delivers the dichroism, while the first term is reflection symmetric. Thus,

$$\Delta(\mathbf{R}_N) = i\mu^* \cdot (\hat{x}\hat{y} - \hat{y}\hat{x}) \cdot \mu = i(\mu^* \times \mu) \cdot \hat{k}_\gamma. \tag{19}$$

Hence, dichroism is characterized by the pseudovector $i\mu^* \times \mu = 2\text{Im}\,\mu \times \text{Re}\,\mu$ generated by the transfer of the photon's chirality to the electron and ion pairs.

To give an idea of the momentum dependence of this general expression, we consider two limiting cases of our approximate dipole moment from equation (7). First, we integrate equation (19) over all ion-axis alignments $\hat{R}_N$ to derive a helium-like dichroism relevant to experiments which might detect only the electron-pair. The integration is straightforward with just the single identity $\int \hat{R}_N \hat{R}_N \, d\hat{R}_N = \frac{4\pi}{3}\mathbf{I}$, and we obtain

$$\int \Delta(\mathbf{R}_N) \frac{d\hat{R}_N}{4\pi} = 2|\tilde{\Lambda}|^2 \,\text{Im}\,(\mathcal{C}_0^* \mathcal{C}_1)\mathbf{k}_r \cdot \hat{k}_R(\hat{k}_R \times \hat{k}_r) \cdot \hat{k}_\gamma$$
$$= \frac{2}{k_R^2}|\tilde{\Lambda}|^2 \text{Im}\,(\mathcal{C}_0^* \mathcal{C}_1)(E_1 - E_2)(\mathbf{k}_1 \times \mathbf{k}_2) \cdot \hat{k}_\gamma$$
$$= \frac{4}{k_R^2}|\tilde{\Lambda}|^2 \text{Im}\,(\mathcal{C}_0^* \mathcal{C}_1)(E_1 - E_2)\sqrt{E_1 E_2} \sin\theta_{\gamma 1} \sin\theta_{\gamma 2} \sin\phi_{\gamma 12}, \tag{20}$$

where we have used $\mathbf{k}_r \cdot \mathbf{k}_R = E_1 - E_2$ and $\mathbf{k}_R \times \mathbf{k}_r = \mathbf{k}_1 \times \mathbf{k}_2$ calculated from equation (1) as well as the polar-angle representation of the momenta $\mathbf{k}_{i=1,2}$ from equation (2) with z axis along $\hat{k}_\gamma$ such that $\phi_{\gamma 12} \equiv \phi_{\gamma 1} - \phi_{\gamma 2}$. Here $\text{Im}\,(\mathcal{C}_0^* \mathcal{C}_1) \equiv \frac{1}{3}\text{Im}\,(c_{\Pi 0}^* c_{\Pi 1} + c_{\Pi 0}^* c_{\Sigma 1} + c_{\Sigma 0}^* c_{\Pi 1})$, which reduces to $\text{Im}\,(c_0^* c_1)$ in the helium-like limit $c_{\Sigma K} \to c_{\Pi K}$. Equation (20) is geometrically identical to the helium dichroism derived by Berakdar and Klar (1992) and studied by Berakdar *et al* (1993), although it differs in the energy-dependent factors $k_R^{-2}|\tilde{\Lambda}(E_1, E_2, \theta_{12})|^2(E_1 - E_2)\sqrt{E_1 E_2}$, which derive from the fourth-order Wannier theory. The result makes clear that a nonvanishing dichroism in helium requires mixed internal K symmetries corresponding to excitations $\mathbf{k}_r$ along $\mathbf{k}_R$ ($K = 0$) and perpendicular to $\mathbf{k}_R$ ($K = 1$) (see also Berakdar 1998, 1999). In addition, it shows that the dichroism is strongest when $\mathbf{k}_r$ and $\mathbf{k}_R$ (or $\mathbf{k}_1$ and $\mathbf{k}_2$) lie in the same plane with ϵ_M, so that $\mathbf{k}_R \times \mathbf{k}_r$ (or $\mathbf{k}_1 \times \mathbf{k}_2$) is parallel to $\hat{k}_\gamma$. As discussed above, the chirality and hence the dichroism vanish when the fragmentation no longer defines three distinct directions and therefore when any of the three vectors $\mathbf{k}_r, \mathbf{k}_R, \hat{k}_\gamma$ (or $\mathbf{k}_1, \mathbf{k}_2, \hat{k}_\gamma$) are parallel.

As a final example, we consider equation (19) for equal energy electrons. This case is interesting because the dichroism vanishes in helium when $E_1 = E_2$ (cf equation (20)). The transition dipole moment μ from equation (7) simplifies considerably when $\mathbf{k}_r \cdot \mathbf{k}_R = 0$, and one easily obtains

$$\Delta(\mathbf{R}_N) = 2|\tilde{\Lambda}|^2 \text{Im}\,(c_{\Pi 1}^* c_{\Sigma 1})\mathbf{k}_r \cdot \hat{R}_N(\hat{R}_N \times \mathbf{k}_r) \cdot \hat{k}_\gamma$$
$$= 2EG(E, \theta_{12})\text{Im}\,(c_{\Pi 1}^* c_{\Sigma 1})(\hat{k}_1 + \hat{k}_2) \cdot \hat{R}_N\left[\hat{R}_N \times (\hat{k}_1 + \hat{k}_2)\right] \cdot \hat{k}_\gamma. \tag{21}$$

Note that here, unlike in helium and in the helium-like result equation (20), only pure $K = 1$ internal excitation enters. To emphasize the role of ion detection, we can integrate this result over $\hat{k}_2$ to correspond to detection of just one electron. (As mentioned already, a nonvanishing dichroism in helium requires detection of both electrons.) The integration is best performed by taking the z axis along k_1, so that the correlation function $G(E, \theta_{12})$ is azimuthally symmetric. It is then straightforward to show that $\int \Delta(\boldsymbol{R}_N) \, d\hat{k}_2 \propto \hat{k}_1 \cdot \hat{\boldsymbol{R}}_N(\hat{\boldsymbol{R}}_N \times \hat{k}_1) \cdot \hat{k}_\gamma \to \frac{1}{2}\sin 2\phi_{\gamma 1}$ for k_1 and $\boldsymbol{R}_N$ separated by the (azimuthal) angle $\phi_{\gamma 1}$ in a plane perpendicular to k_γ. This is in fact the plane defined by our electron-pair analyser, the description of which we now turn to.

4. Experiment

We specialize our molecular electron-pair cross section equation (11) to the case of equal energy sharing $E_1 = E_2 \sim 10$ eV relevant to our experiments and obtain

$$\text{TDCS}[\text{D}_2] \sim \tfrac{4}{15}\pi \left[2|g_\Sigma|^2 + 7|g_\Pi|^2 + 6\text{Re}\,(g_\Pi^* g_\Sigma) \right] (\boldsymbol{\epsilon} \cdot \hat{k}_1 + \boldsymbol{\epsilon} \cdot \hat{k}_2)^2$$
$$+ \tfrac{4}{15}\pi |g_\Sigma - g_\Pi|^2 |\hat{k}_1 + \hat{k}_2|^2. \tag{22}$$

We thus recover the expression derived in Feagin (1998), but now identify $g_\alpha(E_1 = E_2, \theta_{12}) \simeq \sqrt{EG(E, \theta_{12})}\, c_{\alpha 1}$. The first term on the right-hand side of this result is proportional to the equal-energy helium cross section TDCS[He], while the second term is clearly a molecular correction dependent on just the mutual momentum angle, $|\hat{k}_1 + \hat{k}_2|^2 = 4\cos^2\frac{1}{2}\theta_{12}$, independent of the polarization vector $\boldsymbol{\epsilon}$. This change in relative azimuthal symmetry about the polarization axis $\boldsymbol{\epsilon}$ is manifest in a relaxing of selection rules which have been established for *atomic* PDI (Maulbetsch and Briggs 1995). These rules require that the helium TDCS is identically zero in the following situations for a $^1\text{P}^\text{o}$ ($M = 0$) electron-pair final state: (a) when $k_1 \perp \boldsymbol{\epsilon}$ and $k_2 \perp \boldsymbol{\epsilon}$, (b) when $\hat{k}_1 \cdot \boldsymbol{\epsilon} = -\hat{k}_2 \cdot \boldsymbol{\epsilon}$, and (c) when $k_1 = -k_2$†.

Rules (a) and (b) are subtle consequences of parity and exchange symmetry of the electron pair and are clearly relaxed in the presence of the additional axis $\boldsymbol{R}_N$ leading to the molecular correction term in equation (22) independent of $\boldsymbol{\epsilon}$. Rule (b) results in a null first term on the right-hand side of equation (22)—the helium-like contribution—for k_2 anywhere on the conical surface shown in figure 1. Rule (c) on the other hand is a straightforward consequence of parity and exchange symmetry and holds even in the molecule for ungerade, singlet final states. This rule, corresponding to back-to-back electron emission, results in a null molecular cross section along the line $k_2 = -k_1$ on one side of the cone in figure 1. As we have shown (Feagin 1998), the failure of rule (b) in the molecular correction term has measurable consequences in the vicinity of back-to-back emission (i.e. near $\theta_{12} = 180°$ for coplanar detection geometry) due
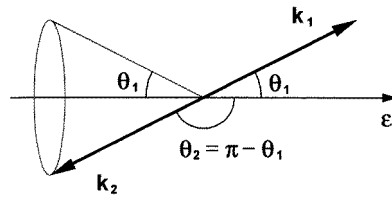
Figure 1. A diagram of the conical surface defined by $\hat{k}_2 \cdot \boldsymbol{\epsilon} = -\hat{k}_1 \cdot \boldsymbol{\epsilon}$ on which the helium TDCS vanishes identically from selection rule (b) discussed in the text. This surface, also given by $\theta_2 = \pi - \theta_1$, includes the exact node from parity and exchange considerations for 'back-to-back' electron emission $\theta_{12} = \pi$.

† Note rule (a) holds for all final electron energies, while rules (b) and (c) hold for equal-energy electrons only.

to the finite detection solid angles resulting in electron collection across a finite portion of the cone defined by rule (b). As we will show here, the lack of a node in the molecular correction term on the opposite side of the cone from $k_2 = -k_1$ (top of the cone in figure 1) also results in a significant increase in the measured molecular TDCS in this angular region in comparison to helium.

For reasons of brevity, the procedures involved in applying the theory to an experimental geometry were only mentioned in Feagin (1998). We therefore present the important details here, not only to make our analysis clear, but also to assist in the theory's application to future measurements. We first consider integration of the cross section equation (22) over the acceptance solid angles defined by our detector. The projections $\epsilon \cdot \hat{k}_i$ in equation (22) are generally expressed as $\cos \theta_i$ in the conventional spherical polar co-ordinate system with z axis along the polarization axis. Our toroidal analysers, however, are axially symmetric about the photon propagation direction k_γ and define a detection 'plane' perpendicular to it (see Reddish *et al* 1997b for full details). Therefore integrals over the acceptance solid angles of the detector are more readily performed in a spherical polar co-ordinate system with z axis along k_γ. Then, electron pairs passing into the detector have polar angles $\theta_{\gamma1} \simeq \theta_{\gamma2} \simeq 90°$ within the range $\pm\frac{1}{2}\delta\theta_\gamma$ defined by the analyser's entrance geometry, which is assumed to be constant for all azimuthal angles $\phi_{\gamma1}$ and $\phi_{\gamma2}$ ($0°$ to $360°$) about k_γ. The geometrical upper limit for $\delta\theta_\gamma$ is $20°$ ($\pm\frac{1}{2}\delta\theta_\gamma = \pm10°$), but electron optical simulations indicate that a somewhat smaller θ_γ-angular acceptance is transmitted through the analyser, somewhere between $14°$ and $20°$ depending on the actual tuning conditions.

We analytically evaluate the $\theta_{\gamma i}$ integrals over the detector slit with a peaking approximation to the Gaussian correlation function $G(E, \theta_{12})$. With $\theta_{\gamma1} = \theta_{\gamma2} = 90°$, the projections $\epsilon \cdot \hat{k}_i = \cos \phi_{\gamma i}$. We thus set $G(E, \theta_{12}) = G(E, |\phi_{\gamma12} \equiv \phi_{\gamma1} - \phi_{\gamma2}|)$ and simply remove it from the integrals. We then obtain for the helium-like contribution $(\epsilon \cdot \hat{k}_1 + \epsilon \cdot \hat{k}_2)^2$ to equation (22)

$$T_1(\phi_{\gamma1}, \phi_{\gamma2}) = (\cos^2 \phi_{\gamma1} + \cos^2 \phi_{\gamma2}) \left[\tfrac{4}{3}(2 + \cos^2 \tfrac{1}{2}\delta\theta_\gamma) \sin^2 \tfrac{1}{2}\delta\theta_\gamma\right]$$
$$+ \tfrac{1}{2} \cos \phi_{\gamma1} \cos \phi_{\gamma2}(\delta\theta_\gamma + \sin \delta\theta_\gamma)^2. \tag{23}$$

As desired, this result reduces to $\delta\theta_\gamma^2(\cos \phi_{\gamma1} + \cos \phi_{\gamma2})^2$ in the small-slit approximation. (Consequently, the $\theta_{\gamma i}$ integrations have little effect on the shape of the angular distributions in helium.) Likewise, we obtain for the $\theta_{\gamma i}$ integrations of the molecular-correction contribution $|\hat{k}_1 + \hat{k}_2|^2 = 4\cos^2 \tfrac{1}{2}\theta_{12}$ to equation (22)

$$T_2(\phi_{\gamma1}, \phi_{\gamma2}) = 2 \sin^2 \tfrac{1}{2}\delta\theta_\gamma + \tfrac{1}{8} \cos(\phi_{\gamma1} - \phi_{\gamma2})(\delta\theta_\gamma + \sin \delta\theta_\gamma)^2. \tag{24}$$

Although we find these analytic $\theta_{\gamma i}$ integrals T_1 and T_2 to be suitably accurate, it was necessary to perform the final $\phi_{\gamma i}$ integrations numerically. Our spectrometer's ϕ_γ angular resolution was quoted in Wightman *et al* (1998) for the data presented there as $\pm2.5°$ with angular 'bins' of $17°$ and $10°$ for the two analysers. The $\phi_{\gamma1}$ and $\phi_{\gamma2}$ integrals for the data presented here have full-widths of $22°$ and $16°$, slightly broader than—but in keeping with—the previously quoted values. They were chosen to reproduce the degree of 'filling-in' of the node in the measured helium angular distributions. We denote T_1 and T_2 integrated over $\phi_{\gamma i}$ as $\bar{T}_1$ and $\bar{T}_2$.

Finally, the quantities $\bar{T}_1$ and $\bar{T}_2$, fully integrated over detection solid angles, can be combined in the usual way to take into account the degree of linear polarization, namely TDCS $\propto \frac{1+S_1}{2}$TDCS$_x$ + $\frac{1-S_1}{2}$TDCS$_y$ in terms of the Stoke's parameter S_1 (Schwarzkopf *et al* 1993).

The ratio of angular distributions $\overline{\text{TDCS}}[D_2]/\overline{\text{TDCS}}[\text{He}]$ emphasizes their difference, which as figure 2(*a*) demonstrates is most pronounced in the region $\theta_{12} = 180°$. This peak in the ratio occurs in an angular range where TDCS$[D_2]$ and TDCS$[\text{He}]$ are both very small, as
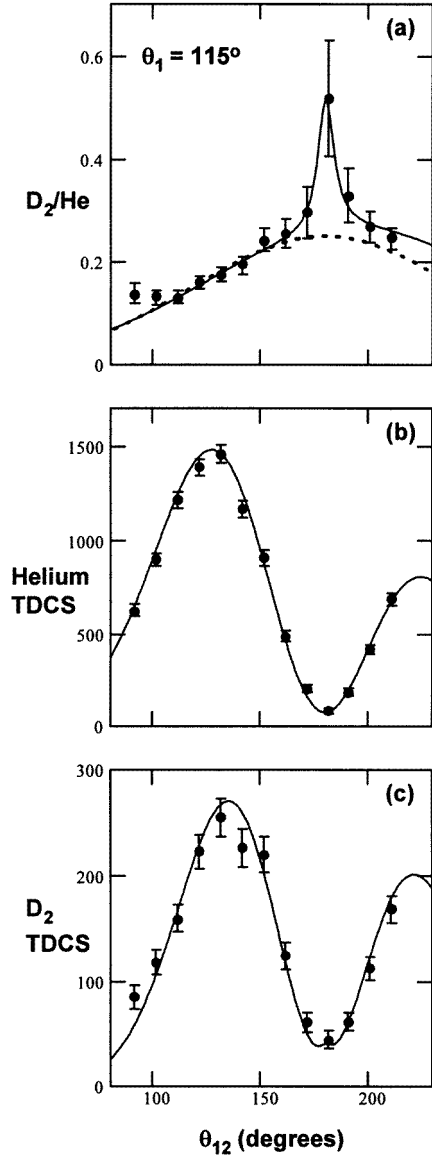
Figure 2. (*a*) Ratio of the D_2-to-He coincidence yield as a function of the electron-pair mutual momentum angle θ_{12} from the data of Wightman *et al* (1998) for $\theta_1 = 115°$. The solid curve shows the corresponding ratios computed from the theoretical fits from equation (25). The dotted curve under the peak shows the ratio of the two Gaussian correlation functions used for D_2 and He. (*b*) The helium and (*c*) the D_2 TDCS data from Wightman *et al* (1998) with $E_1 = E_2 \simeq 10$ eV and Stoke's parameter $S_1 = 0.67 \pm 0.03$. The helium fit includes a Gaussian correlation function with half-width $\theta_{1/2} = 91° \pm 3°$. The D_2 fit is from equation (22) with a ratio $\eta = g_\Pi/g_\Sigma = -2.1$ and correlation function half width $\theta_{1/2} = 76° \pm 3°$. Both fits include integration over detection solid angles, as discussed in the text.

figures 2(*b*) and (*c*) show, which explains the relatively large error bars. Collecting results, we can express this ratio as

$$\frac{\overline{\overline{TDCS}}[D_2]}{\overline{\overline{TDCS}}[He]} \sim \frac{G_{D_2}(|\phi_{\gamma 12}|)}{G_{He}(|\phi_{\gamma 12}|)} \left[1 + C(\eta) \frac{\bar{T}_2(\phi_{\gamma 1}, \phi_{\gamma 2})}{\bar{T}_1(\phi_{\gamma 1}, \phi_{\gamma 2})} \right], \tag{25}$$

where $\phi_{\gamma 12} \equiv \phi_{\gamma 1} - \phi_{\gamma 2}$ and $\eta \equiv g_\Pi/g_\Sigma = c_{\Pi 1}/c_{\Sigma 1}$ with

$$C(\eta) \equiv \frac{4|1-\eta|^2}{2 + 7|\eta|^2 + 6\operatorname{Re}\eta}. \tag{26}$$

Note that when $\eta = 1$ corresponding to $g_\Pi = g_\Sigma$, $C(1) = 0$ and the molecular-correction term vanishes from equation (25), leaving us with simply the ratio of the two Gaussian correlation

functions. The quantities η and $C(\eta)$ are generally complex valued, although we assume both to be real here for simplicity. Using all three data sets $\theta_1 = 98°$, $115°$, and $132°$ from Wightman *et al* (1998) and the $\phi_{\gamma i}$-angular acceptances given above, we obtain a best fit to the ratio data in figure 2(*a*) with $\delta\theta_\gamma = 18° \pm 1°$ and $C(\eta) = -1.9 \pm 0.4$, which corresponds to $\eta = -2.1 \pm 0.5$ or $\eta = +0.01 \pm 0.05$†. These values were used to produce the other curves in figure 2.

We can also relate the ratio η to the ion angular asymmetry parameter from equation (13) via the approximation

$$\beta_N \simeq \frac{2(1 - |\eta|^2)}{1 + |\eta|^2} \qquad \text{or} \qquad |\eta|^2 \simeq \frac{2 - \beta_N}{2(1 + \beta_N)}, \tag{27}$$

where we have assumed that $\frac{1}{2}|c_{\alpha 0}/c_{\alpha 1}|^2 \ll 1$, since analysis of helium data for $E = 20$ eV has shown that $c_0/c_1 \sim \frac{1}{3}$ (Dörner *et al* 1998a). Thus, the value $\eta = +0.01 \pm 0.05$ determined in the above fit implies a negligible g_Π amplitude with $\beta_N \simeq +2$, values which are inconsistent with the ion distributions measured by Kossmann *et al* (1989), who obtained the result $\beta_N = -0.71 \pm 0.05$ at a photon energy of 71 eV. (Dörner *et al* 1998b obtained the value $\beta_N = -0.60 \pm 0.05$ at a photon energy of 58.8 eV.) However, the other value $\eta = -2.1 \pm 0.5$ determined in the above fit corresponds to $\beta_N = -0.69 \pm 0.13$, which is in good agreement with the Kossmann result. We find this correspondence satisfactory despite the approximations, as a more accurate fit by the above procedure would be inherently difficult because the analysis depends on the ratio of two 'null' signals. This demonstrates that within the assumptions of our approximation, one can use the measured β_N values to determine the ratio g_Π/g_Σ at different photon energies. The ratio peaks around $+2.3$ for photon energies near the nominal double ionization threshold of 51.1 eV and gradually falls off at higher photon energies to about $+1.5$ at 100 eV. This trend might serve as a rough prediction for future $(\gamma, 2e)$ measurements and it will be interesting to compare them with future theoretical and experimental studies of both equal and unequal electron energy sharing.

Arguably, the most important evidence in support of our description comes from examining other consequences of the molecular-correction term in the TDCS. Given a ratio of $g_\Pi/g_\Sigma \simeq -2.1$ with our kinematic conditions, we can use equation (22) (which includes the assumption that the correlation half-width $\theta_{1/2}$ is the same for both g_Π and g_Σ amplitudes) to examine the shape of the TDCS at other θ_1 ($= \phi_{\gamma 1}$) angles. The amplitudes of the two characteristic lobes are a sensitive function of θ_1 as well as of the degree of linear polarization S_1. The effect of the molecular correction term is to dramatically alter the relative intensity of the two lobes as a function of θ_1 in comparison to that of helium. This is particularly evident at $\theta_1 = 144°$, an angle where the TDCS had been measured earlier (Reddish *et al* 1997a). The comparison of the TDCS, using both atomic and molecular descriptions but with the same correlation function half-widths $\theta_{1/2} = 76°$, is shown in figures 3 and 4.

Figure 3(*a*) shows a polar plot of the Gaussian correlation function G with a 76° half-width along with the He and D_2 angular functions defined by $\overline{\text{TDCS}}[\text{He}]/G$ and $\overline{\text{TDCS}}[D_2]/G$. The helium distribution is symmetric about the polarization axis while the D_2 distribution is clearly skewed by the additional molecular correction term. The product of the correlation function and the two angular functions is shown in figure 3(*b*). The marked increase in amplitude of the smaller lobe along the polarization direction is a consequence of the relaxation of the selection rules we have discussed. As seen in figure 4, this prediction is in good agreement with earlier data, which were taken with $S_1 = 0.67 \pm 0.03$. This supporting evidence for our

---

† Note η as function of C is double valued, and we therefore include the $\eta > 0$ value, although our own partial-wave analysis indicates that $\eta < 0$ is expected.
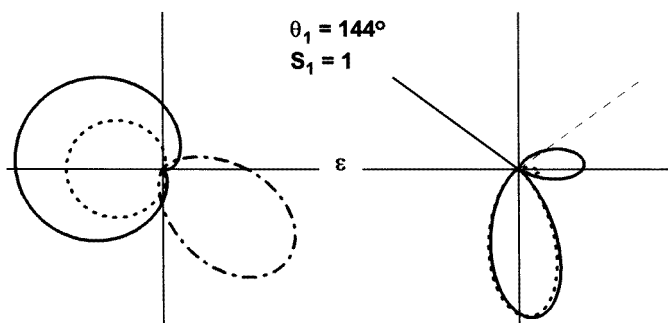
Figure 3. (*a*) A polar plot for $\theta_1 = \phi_{\gamma 1} = 144°$ of the Gaussian correlation function $G(E, |\phi_{\gamma 1} - \phi_{\gamma 2}|)$ with half-width $\theta_{1/2} = 76°$ (dash-dot) and the helium (dot) and D_2 (solid) angular distributions defined by $\overline{TDCS}[He]/G$ and $\overline{TDCS}[D_2]/G$. With an amplitude ratio $g_\Pi/g_\Sigma = -2.1$, the D_2 function no longer has symmetry about the polarization axis along the horizontal. (*b*) A polar plot of the product of the angular distributions and the correlation function with 76° half-width for D_2 (solid) and He (dots), representing the TDCS with 100% linear polarization. The solid line indicates the θ_1 angle and the dashed line shows the position of the extra node in helium which effectively suppresses the TDCS between $\phi_{\gamma 2} = \pi \pm \phi_{\gamma 1}$.
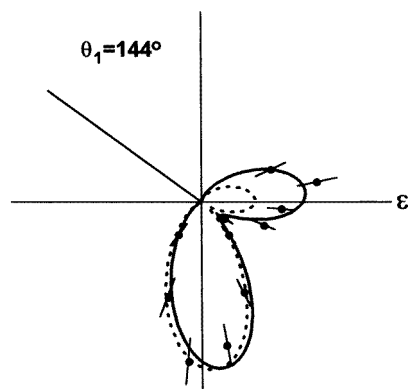
Figure 4. Measured $(\gamma, 2e)$ D_2 TDCS for $E_1 = E_2 \sim 10$ eV with Stoke's parameter $S_1 = 0.67 \pm 0.03$ from Reddish *et al* (1997a). The solid and dotted curves are the molecular and atomic forms of the $\overline{TDCS}$, respectively, with the same 76° correlation-function half-width. Both curves include integration over detection solid angles and are normalized at their peak values.

molecular photofragmentation description also suggests that the correlation half-width is not too dissimilar for the g_Π and g_Σ amplitudes at these kinematic conditions.

5. Conclusion

We have presented a helium-like description of PDI of molecular deuterium—or hydrogen—for both linearly and circularly polarized photons and therefore for circular dichroism in the angular distribution of the ions and electrons. Our simple approach affords an angle-free representation of the cross section that exhibits explicitly its dependence on the electron momenta and the ion-axis orientation, as well as the amplitudes g_Σ and g_Π for electron-pair excitation parallel and perpendicular to the molecular axis. By connecting with a fourth-order Wannier description of the electron-pair continuum wavefunction, we derive an approximate dependence of these amplitudes on electron energy sharing and a dynamical quantum number K to classify the internal excitations of the electron pair. The description has thus shown considerable consistency with recent $(\gamma, 2e)$ and ion-electron experiments.

Our model is based on the dominant (95.6%) S^e component of the molecular ground state

and neglects entirely higher-order multipoles, although experimental observations to date do not rule them out and recent calculations by Walter and Briggs (1999) show evidence for them with small additional structures in the TDCS. Their 5C calculations of the fragmenting four-particle molecular state are in full analogy with 3C calculations of helium PDI and are likely to become the 'virtual reality' of molecular PDI. The higher-order multipoles may also account for the observed narrowing of the characteristic lobes in the angular distributions, also seen in the results of Walter and Briggs. While our model's angle-independent simplicity might survive inclusion of the next strongest (2.6%) D^e component, systematic inclusion of higher multipoles would likely require a more traditional approach involving a full partial-wave analysis.

We have assumed that the correlation function half-width $\theta_{1/2}$ is the same for both amplitudes g_Σ and g_Π. Although this approximation seems acceptable when examining the shape of the angular distribution in the vicinity of the node at $\theta_{12} = \pi$, where the correlation functions are peaked, it becomes questionable when considering the overall shape of the TDCS. Extensions of our description might therefore include construction of a Wannier wavefunction for an ion pair with the ground-state separation of the molecule and an electron pair with outgoing components parallel and perpendicular to the ion axis.

Acknowledgments

References

Berakdar J 1998 *J. Phys. B: At. Mol. Opt. Phys.* **31** 3167
——1999 *J. Phys. B: At. Mol. Opt. Phys.* **32** L27
Berakdar J and Klar H 1992 *Phys. Rev. Lett.* **69** 1175
Berakdar J, Klar H, Huetz A and Selles P 1993 *J. Phys. B: At. Mol. Opt. Phys.* **26** 1463
Bishop D M 1963 *Mol. Phys.* **6** 305
Dehmer J L and Dill D 1978 *Phys. Rev.* A **18** 164
Dörner R *et al* 1998a *Phys. Rev.* A **57** 1074
——1998b *Phys. Rev. Lett.* **81** 5776
Dujardin G, Besnard M J, Hellner L and Malinovitch Y 1987 *Phys. Rev.* A **35** 5012
Feagin J M 1995 *J. Phys. B: At. Mol. Opt. Phys.* **28** 1495
——1996 *J. Phys. B: At. Mol. Opt. Phys.* **29** L551
——1998 *J. Phys. B: At. Mol. Opt. Phys.* **31** L729
Huetz A, Andric L, Jean A, Lablanquie P, Selles P and Mazeau J 1995 *XIX Int. Conf. on Physics of Electronic and Atomic Collisions, Invited Talk (AIP Conf. Proc. 139)*
Huetz A, Selles P, Waymel D and Mazeau J 1991 *J. Phys. B: At. Mol. Opt. Phys.* **24** 1917
Joy H W and Parr R G 1958 *J. Chem. Phys.* **28** 448
Kazansky A K and Ostrovsky V N 1995 *Phys. Rev.* A **51** 3698
Kossmann H, Schwarzkopf O, Kämmerling B and Schmidt V 1989 *Phys. Rev. Lett.* **63** 2040
Lablanquie P, Mazeau J, Andric L, Selles P and Huetz A 1995 *Phys. Rev. Lett.* **74** 2192
LeRouzo H 1986 *J. Phys. B: At. Mol. Phys.* **19** L677
——1988 *Phys. Rev.* A **37** 1512
Maulbetsch F and Briggs J S 1993 *J. Phys. B: At. Mol. Opt. Phys.* **26** L647
——1995 *J. Phys. B: At. Mol. Opt. Phys.* **28** 551
Mergel V *et al* 1998 *Phys. Rev. Lett.* **80** 5301
Pont M and Shakeshaft R 1995 *J. Phys. B: At. Mol. Opt. Phys.* **28** L571

——1995 *Phys. Rev.* A **51** R2676

Reddish T J, Richmond G, Bagley G W, Wightman J P and Cvejanović S 1997b *Rev. Sci. Instrum.* **68** 2685

Reddish T J, Wightman J P, MacDonald M A and Cvejanović S 1997a *Phys. Rev. Lett.* **79** 2438

Scherer N, Lörch H and Schmidt V 1998 *J. Phys. B: At. Mol. Opt. Phys.* **31** L817

Schwarzkopf O, Krässig B, Elmiger J and Schmidt V 1993 *Phys. Rev. Lett.* **70** 3008

Viefhaus J *et al* 1996 *Phys. Rev. Lett.* **77** 3975

Walter M and Briggs J S 1999 *J. Phys. B: At. Mol. Opt. Phys.* **32** 2487

Wightman J P, Cvejanović S and Reddish T J 1998 *J. Phys. B: At. Mol. Opt. Phys.* **31** 1753

Zare R N 1988 *Angular Momentum* (New York: Wiley–Interscience)